

# Generalist Vision Foundation Models for Medical Imaging: A Case Study of Segment Anything Model on Zero-Shot Medical Segmentation

Peilun Shi<sup>†</sup>Jianing Qiu<sup>†,‡</sup>Sai Mu Dalike Abaxi<sup>†</sup>Hao Wei<sup>†</sup>Frank P.-W. Lo<sup>‡</sup>Wu Yuan<sup>†,\*</sup><sup>†</sup>The Chinese University of Hong Kong<sup>‡</sup>Imperial College London{peilunshi, tariqabaxi, wyuan}@cuhk.edu.hk  
haowei@link.cuhk.edu.hk

{jianing.qiu17, po.lo15}@imperial.ac.uk

## Abstract

We examine the recent Segment Anything Model (SAM) on medical images, and report both quantitative and qualitative zero-shot segmentation results on nine medical image segmentation benchmarks, covering various imaging modalities, such as optical coherence tomography (OCT), magnetic resonance imaging (MRI), and computed tomography (CT), as well as different applications including dermatology, ophthalmology, and radiology. Our experiments reveal that while SAM demonstrates stunning segmentation performance on images from the general domain, for those out-of-distribution images, e.g., medical images, its zero-shot segmentation performance is still limited. Furthermore, SAM demonstrated varying zero-shot segmentation performance across different unseen medical domains. For example, it had a 0.8704 mean Dice score on segmenting under-bruch's membrane layer of retinal OCT, whereas the segmentation accuracy drops to 0.0688 when segmenting retinal pigment epithelium. For certain structured targets, e.g., blood vessels, the zero-shot segmentation of SAM completely failed, whereas a simple fine-tuning of it with small amount of data could lead to remarkable improvements of the segmentation quality. Our study indicates the versatility of generalist vision foundation models on solving specific tasks in medical imaging, and their great potential to achieve desired performance through fine-tuning and eventually tackle the challenges of accessing large diverse medical datasets and the complexity of medical domains.

## 1. Introduction

Recently, large AI models (LAMs) have been actively researched as they manifest impressive performance on various downstream tasks and offer a foundation to advance and

foster future research in manifold AI areas, such as computer vision and natural language processing [4]. In medical and healthcare domains, LAMs are also transforming methodological designs and paradigms, and establishing new state-of-the-arts and breakthroughs in various sectors including medical informatics and decision-making [26]. Despite the active development, advances in medical LAMs often lag behind their counterparts in general domains. To identify current discrepancies and guide the future development of medical LAMs, we select one of these LAMs in the general domain, i.e., Segment Anything Model (SAM) [20], which is a foundational vision model recently proposed for image segmentation and has shown stunning performance on tasks ranging from edge detection to instance segmentation, and thoroughly evaluate its zero-shot segmentation performance on medical images. Although there are few studies out there that tested SAM on medical imaging, they either only focus on one imaging modality, i.e., pathology [11], or only showcase a few qualitative segmentation samples [18] without reporting quantitative results. To provide a comprehensive and objective evaluation of SAM on medical image segmentation, this work conducted extensive experiments on nine benchmarks using the zero-shot segmentation feature of SAM. The selected datasets contain a wide diversity of medical imaging modalities and organs.

Our key findings include:

1. SAM demonstrated better performance on endoscopic and dermoscopic images than other medical modalities, which is conjectured as SAM was trained with a large volume of RGB image data, and endoscopic and dermoscopic images are essentially images captured by RGB cameras. Therefore, when transferred to relevant medical images, SAM can demonstrate a relatively decent and consistent performance as it is tested on general RGB images.
2. SAM failed to carry out zero-shot segmentation tasks

\*Corresponding author

on images that have continuous branching structures, such as blood vessels. Interestingly enough, when tested on images of tree branches, we found SAM was actually also unable to segment them in a zero-shot manner.

3. Compared to models specially designed for medical imaging, the zero-shot segmentation capability of SAM on medical images are decent but often inferior to those domain-specific models. Our experiments reveal that the Dice coefficients of SAM on medical benchmarks were generally lower by 0.1-0.4 compared to previous state-of-the-art (SOTA) models in medical image segmentation. In the worst case, the Dice score of the zero-shot SAM is even lower than the SOTA by 0.65.
4. Preliminary experiments of fine-tuning SAM were conducted. A simple fine-tuning of SAM on small amount of retinal vessel data led to impressive improvements of the segmentation quality, implying the great potential of SAM on medical image segmentation by fine-tuning.

## 2. Segment Anything Model

SAM is a generalist vision foundation model for image segmentation, and supports a diverse range of input prompts to enhance the segmentation quality. However, SAM does not recognize the type of each individual segmented object. To facilitate comparison and evaluation, the prompt for segmenting each instance is derived from the centroid of each individual ground truth mask of that instance in our study. Upon receiving the prompt, SAM generates three potential segmentation results and provides corresponding scores. The highest-scored result is selected and compared with the ground truth for evaluation. The details of implementation are introduced in Algorithm 1.

## 3. Experiments

Our study was implemented on a single NVIDIA RTX 3080 GPU and the official checkpoint of ViT-H SAM model was chosen to test the best performance of SAM on zero-shot medical image segmentation. After conducting tests across multiple medical imaging modalities, we observed that the segmentation outcomes were not consistently satisfactory among those modalities.

### 3.1. Medical Image Segmentation Datasets

Nine datasets, including Skin Lesion Analysis Toward Melanoma Detection [10, 32], Drishiti-GS [29], RIM-ONE-r3 [14], REFUGE [24], AMOS [19], MICCAI 2017 Robotic Instrument Segmentation [2], Chest X-ray [5, 15], Rat Colon [25] and AROI [22] (summarized in Table 1), were

---

### Algorithm 1: SAM on Zero-Shot Medical Image Segmentation

---

**Input:** Pretrained SAM Model  $\theta(\cdot, \cdot)$ , contour detector  $CD(\cdot)$ , midpoint detector  $MD(\cdot)$ , medical image dataset  $I$  with labels of classes  $C$ .

**Output:** Segmentation mask set  $M$ .

```

for  $i \in I$  do
  for  $cls \in C$  do
     $i_c \leftarrow (label(i) == cls)$ 
     $Contours \leftarrow CD(i_c)$ 
    Initialize image mask  $m$ 
    for  $c \in Contours$  do
       $P \leftarrow MD(c)$ 
       $m_{outs}, scores \leftarrow \theta(i, P)$ 
       $m \leftarrow Argmax(scores(m_{outs}))$ 
    end
     $M.append(m)$ 
  end
end

```

---

used to examine the performance of SAM on medical image segmentation, covering a wide range of medical imaging modalities, such as OCT, MRI, and CT, as well as a diverse range of organs, including eyes, colon, spleen, kidney, gallbladder, esophagus, liver, and stomach.

### 3.2. Evaluation Metrics

To assess the zero-shot segmentation capability of SAM on medical images, two quantitative metrics were employed: Dice similarity coefficient and Intersection over Union (IoU). The Dice coefficient measures the overlap between two sets of data and ranges from 0 (no overlap) to 1 (perfect overlap). Similarly, IoU computes the ratio of the intersection over the union of two sets and ranges from 0 to 1. Both metrics were then averaged across multiple samples to obtain an overall measure of the segmentation accuracy. Specifically, the Dice coefficient and IoU were calculated as

$$Dice = \frac{2|Y \cap \hat{Y}|}{|Y| + |\hat{Y}|} \quad (1)$$

$$IoU = \frac{|Y \cap \hat{Y}|}{|Y| + |\hat{Y}| - |Y \cap \hat{Y}|} \quad (2)$$

Where  $Y$  refers to the ground truth mask and  $\hat{Y}$  denotes the predicted mask of SAM based on the prompt (i.e., the centroid of the ground truth mask).

Table 1. Datasets Used for Examining the Zero-Shot Medical Image Segmentation Performance of SAM

Dataset	Modality	Details	Number of Test Samples
Skin Lesion Analysis Toward Melanoma Detection [10, 32]	Dermoscope	Skin	259 & 1000
Drishiti-GS [29] RIM-ONE-r3 [14] REFUGE [24]	Fundus	Eye	51 & 60 & 160
AMOS [19]	CT	Abdominal organs	15361
AMOS [19]	MRI	Abdominal organs	3176
MICCAI 2017 Robotic Instrument Segmentation [2]	Endoscope	Tissue	1200
Chest X-ray [5, 15]	X-ray	Chest	704
Rat Colon [25]	Endoscopic OCT	Colon	130
AROI [22]	SD-OCT	Retina	113

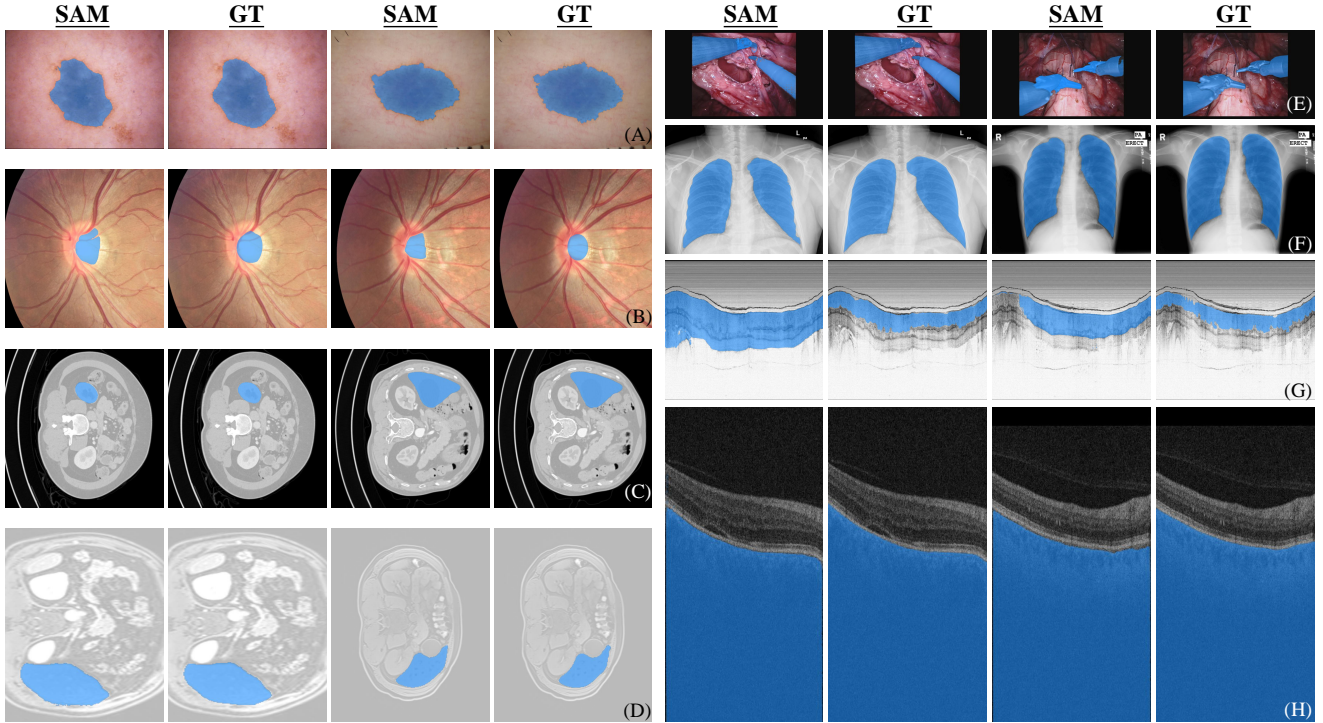


Figure 1. Successful medical segmentation examples of SAM. Eight distinct modalities labeled with (A)-(H) are included, corresponding to dermoscope, fundus, CT, MRI, RGB endoscope, X-Ray, endoscopic OCT and spectral domain OCT. Each set of images comprises four images, containing two pairs of SAM segmentation and ground truth.

### 3.3. Results

#### 3.3.1 Dermoscopic Images

Skin lesion analysis dataset is sourced from the challenge hosted by the International Skin Imaging Collaboration (ISIC) [10, 32]. Note that images captured by dermatoscopes with professional lighting and better magnification always present accurate details and precise contours. However, melanoma appears heterogeneously on different states of skin or diseases. Results are summarized in Table 2 for comparison. From the bottom two rows of Table 2, it is evident that for the same task, there is a significant difference in the final results due to a four-fold difference in the num-

ber of tested samples. We hypothesize that this discrepancy may be attributed to the increased presence of outlier data in the randomly selected smaller sample, resulting in greater randomness in the testing process. Therefore, conducting further testing with larger samples may yield more reliable results. Additionally, as shown in Table 2, the results of SAM are not competitive compared to existing methods. Specifically, SAM (259) denotes the outcome obtained by utilizing ten percent of randomly selected instances from the whole training dataset as a testing subset, which facilitates a straightforward comparison with existing methods. On the other hand, SAM (1000) refers to the performance of the model assessed on the official complete testing dataset.

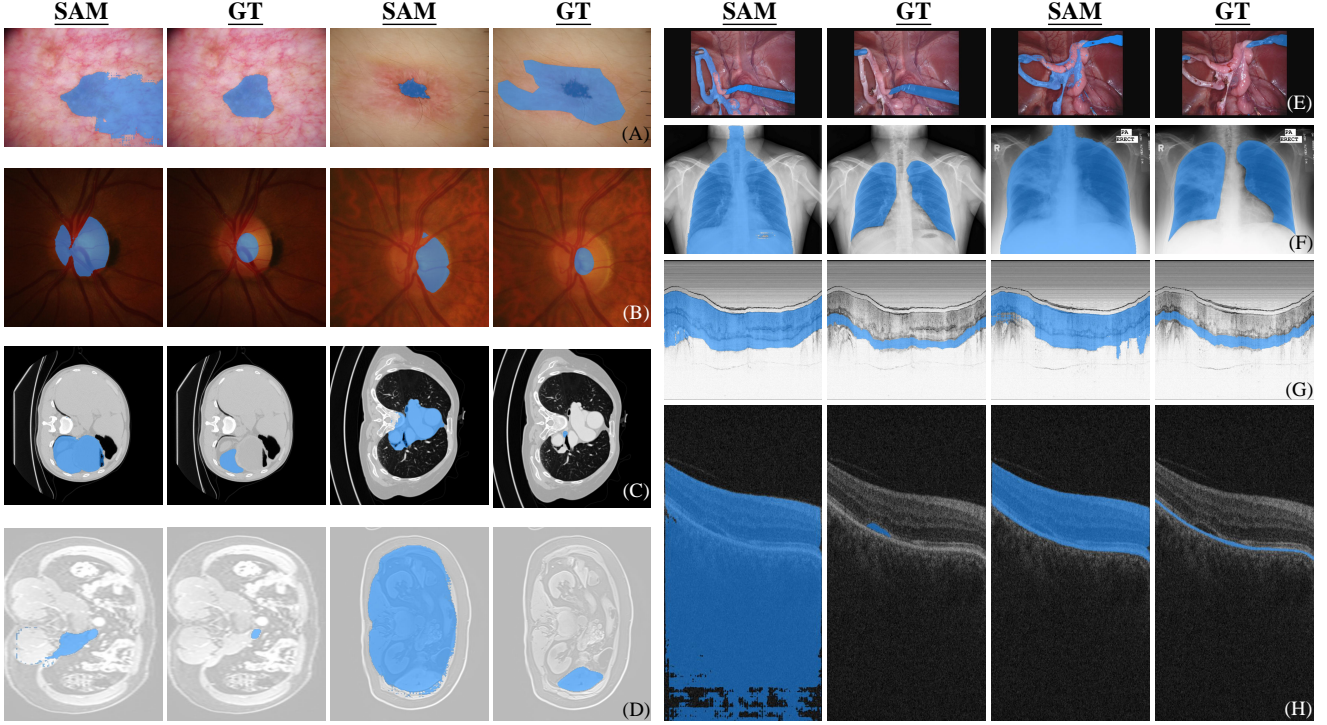


Figure 2. Failure medical segmentation examples of SAM. Eight distinct modalities labeled with (A)-(H) are included, corresponding to dermoscope, fundus, CT, MRI, RGB endoscope, X-Ray, endoscopic OCT and spectral domain OCT. Each set of images comprises four distinct images, containing two pairs of SAM segmentation and ground truth.

Figure 1 (A) shows two samples that SAM perfectly segmented. As shown in Figure 1 (A), SAM is able to accurately segment the target when the anomalous regions are positioned at the center and exhibit a distinct morphology.

Figure 2 (A) shows two failure cases. When the target lesion appeared within the erythematous or scars, the segmentation often fails due to the similarity of features between the target and the adjacent parts or the absence of clear boundaries (or in another word, the lesion is less obtrusive or apparent).

### 3.3.2 Fundus Images

Retinal fundus images are considered as the primary modality in ophthalmic diagnosis. Specifically, optic cup (OC) and optic disc (OD) segmentation from the fundus image is the essential part. DoFE [34] is a benchmark for OC and OD segmentation that comprises three different fundus image datasets. Due to the small size of available fundus image datasets, we amalgamated the data used in DoFE to evaluate the performance of SAM. Apart from an overall evaluation, we also explored and examined the domain generalization of SAM based on the same domain partitions as DoFE.

Note that OC constitutes a whitish, cup-shaped area situated at the center of the OD, which can be approximated

Table 2. Comparison with the State-of-the-Art Methods on the Skin Lesion Analysis Toward Melanoma Detection Dataset

Method	Dice	IoU
U-Net [27]	0.8550	0.7850
UNet++ [39]	0.8090	0.7290
CaraNet [21]	0.8700	0.782
PraNet [13]	0.8750	0.7870
TransUNet [8]	0.8800	0.8090
TransFuse [38]	0.9010	0.840
Double-UNet [16]	0.8962	0.8212
Polyp-PVT [12]	0.8962	0.8212
DuAT [30]	0.9230	0.8670
Polar Res-U-Net++(SOTA) [3]	<b>0.9253</b>	<b>0.8743</b>
SAM (259 samples, common practice)	0.6636	0.5566
SAM (1000 samples, official test set)	0.7306	0.6169

as two concentric circles of different radius. Specifically, the fundus images were cropped to better observe the region of interest (ROI). The positions of the two prompts exhibit a high degree of proximity, occasionally coinciding with each other. Thus, accurately segmenting between OC and OD is not easy when receiving similar prompts. This partly causes zero-shot SAM to only have half of the ac-



curacy of the current SOTA. We hypothesize that manually prompting SAM (i.e., like oracle) may lead to accuracy increase but the zero-shot mode of SAM may still lag behind SOTA by a noticeable margin.

We also investigated the performance of SAM on cross-domain scenarios following the setting in DoFE [34]. The imbalanced performance observed in Table 3 demonstrates that the domain generalization (DG) problem also exists in SAM. SAM achieves the best and worst mean performance on domain 1 and domain 4 (18.1 percent difference), respectively. By inspecting fundus images from four domains, we found that the contrast between OC/OD and background is proportional to the final performance. However, this proportional relationship cannot be observed in DG-optimized algorithms in Table 3. This comparison reveals that SAM mainly focuses on superficial features (image contrast) instead of high-level semantics when zero-shot segmenting OC/OD from fundus images.

### 3.3.3 Endoscopic OCT

The OCT Rat Colon dataset [25] was used, which was captured by an 800-nm ultrahigh-resolution endoscopic SD-OCT system [35]. The colonic wall is composed of three distinct layers for segmentation, namely the colonic mucosa (CM), submucosa (SM), and muscularis externa (ME). A tenth of the dataset was randomly sampled in our experiment to evaluate the performance of SAM. Images in this dataset do not contain much color information and complex scenes, which is supposed to be easy for segmentation. Nevertheless, the zero-shot segmentation performance of SAM on endoscopic OCT is far inferior to models designed for medical images as shown in Table 4. Figure 1 (G) and Figure 2 (G) show some segmentation samples of SAM. It can be observed that compared to successful examples of other datasets, the successful examples of endoscopic OCT are actually not perfect, and the failure cases are indeed unsatisfactory.

### 3.3.4 SD-OCT

Annotated Retinal OCT Images Database (AROI) [23] contains 1136 annotated B-scans and associated raw high-resolution images from 24 patients with age-related macular degeneration (AMD). An ophthalmologist annotated three retinal layers and three retinal fluids in each B-scan. The official annotations for B-scan content segmentation involve an eight-category classification task, which includes layers such as the inner plexiform layer and inner nuclear layer (IPL/INL), as well as regions above internal limiting membrane (ILM) and under bruch’s membrane (BM), presenting an easily observable coherent and extensive area. Pigment epithelial detachment (PED), subretinal fluid and subretinal hyperreflective material (SRF), and intraretinal fluid (IRF)

are also involved for segmentation. We did not take the top layer (above ILM) into the consideration (i.e., not tested), because photography is not a part of the organism’s internal structure.

As shown in Table 5, the segmentation result on under BM is much higher than other classes and is also confirmed in the corresponding Figure 1 (H). SAM accurately segmented the layer structure (under BM) which has clear boundaries and large continuous areas. However, the zero-shot segmentation performance of SAM was extremely unsatisfactory for small holes or continuously irregular elongated structures as shown in Figure 2 (H).

### 3.3.5 CT

AMOS [19] contains both CT and MRI modalities for abdominal multi-organ segmentation tasks. The entire dataset introduces 500 CT and 100 MRI volume data from 15 organs in abdominal cavity. During pre-processing, we set the CT window range to [-991, 362] HU and, 15361 slices from the dataset were generated under this standard. Since the corresponding ground truth for the test set has not been released, we chose to conduct a case study on the validation set that contains corresponding segmentation labels. Fifteen organs were segmented, including spleen, right kidney, left kidney, gallbladder, esophagus, liver, stomach, aorta, inferior vena cava, pancreas, right adrenal gland, left adrenal gland, duodenum, bladder, prostate and uterus. The above described are also applied to MRI, and we will discuss the CT experimental results along with MRI in the next section.

### 3.3.6 MRI

The pre-processing method of MRI data is congruent with the one used for CT data mentioned in the preceding section. A total of 3176 images originating from the validation set were obtained and selected for our case study. As the datasets of the two modalities were derived from the same dataset and the 3D data was pre-processed in the same way, the average Dice scores of the two modalities are close, but note that the variations exist across individual class segmentation tasks. As the successful segmentation examples shown in Figure 1 (C) and (D), SAM can accurately perform segmentation for two-dimensional organs from CT and MRI images. The resulting segmented regions manifest precise localization, clear demarcations and a striking resemblance to the actual organ structures in terms of visual appearance. However, failure cases shown in Figure 2 (C) and (D) are often from the segmentation of small organs, in which SAM exhibits a tendency to segment not only the target organ itself but also the neighboring tissues.

Table 3. Comparison with the State-of-the-Art Methods on Fundus Datasets Evaluated using the Dice Similarity Coefficient

Method	Domain 1		Domain 2		Domain 3		Domain 4		Mean
	OC	OD	OC	OD	OC	OD	OC	OD	Total
U-Net [27]	0.7703	0.9496	0.7821	0.8969	0.8028	0.8933	0.8474	0.9009	0.8554
Mixup [36]	0.7332	0.9297	0.7112	0.8678	0.8216	0.9042	0.8623	0.9076	0.8423
DST [37]	0.7563	0.9220	<b>0.8080</b>	0.9077	0.8432	<b>0.9402</b>	0.8624	0.9066	0.8683
JiGen [6]	0.8081	0.9503	0.7946	0.9047	0.8265	0.9194	0.8430	0.9106	0.8697
DoFE [34]	<b>0.8359</b>	<b>0.9559</b>	0.8000	<b>0.9837</b>	<b>0.8666</b>	0.9198	<b>0.8704</b>	<b>0.9332</b>	<b>0.8844</b>
SAM	0.5710	0.5563	0.5200	0.3333	0.5830	0.4157	0.3598	0.4056	0.4609

Table 4. Comparison with the State-of-the-Art Methods on OCT Rat Colon Dataset

Method	Class	Dice	IoU
TransUNet [8]	All	<b>0.9265</b>	-
LiDeOCTNet [1]	All	0.9198	-
SAM	Colonic Mucosa	0.3491	0.2350
	Submucosa	0.2477	0.1485
	Muscularis Externa	0.2399	0.1466
	All	0.2789	0.1767

Table 5. Zero-Shot Segmentation Results of SAM on Different Classes in AROI Dataset

Class	Dice	IoU
ILM-IPL/INL	0.2378	0.1527
IPL/INL-RPE	0.4499	0.3153
RPE-BM	0.0688	0.0368
under BM	<b>0.8704</b>	<b>0.7806</b>
PED	0.1083	0.0673
SRF	0.1084	0.0656
IRF	0.0923	0.0548
Average	0.3237	0.2506

### 3.3.7 X-Ray

The data (704 labelled images) used for testing SAM on X-Ray were derived from the validation and training sets of [5, 15]. As shown in Figure 1 (F), the segmentation performance demonstrated by SAM in successful cases is impressive, and perfectly match with the ground truth segmentation. However, the failure cases shown in Figure 2 (F) revealed that the zero-shot chest X-ray segmentation of SAM was not always consistent. Table 8 shows the quantitative results of zero-shot X-Ray image segmentation.

Table 6. Zero-Shot Segmentation Results of SAM on Different CT Organ Classes in AMOS Dataset

Class	Dice	IoU
#1	0.1616	0.1026
#2	0.2723	0.2211
#3	<b>0.3465</b>	<b>0.2856</b>
#4	0.0943	0.0630
#5	0.1023	0.0724
#6	0.3188	0.2097
#7	0.2624	0.1812
#8	0.2946	0.2310
#9	0.1555	0.1188
#10	0.1375	0.0930
#11	0.0287	0.0202
#12	0.0585	0.0454
#13	0.1831	0.1284
#14	0.1292	0.0752
#15	0.0653	0.0360
Average	0.2105	0.1548

### 3.3.8 Endoscopic Images

We also tested SAM with MICCAI 2017 Robotic Instrument Segmentation dataset [28], which contains 2040 stereo camera images acquired from a da Vinci Xi surgical system on three types of segmentation task (binary, parts and instruments segmentation). The images were essentially captured by RGB cameras. As a result, the segmentation outcomes shown in Figure 1 (E) are impressive when given appropriate prompts. As we placed the prompt at the center of each individual object, a three-class segmentation of parts is the most suitable choice for testing in order to avoid any irregular connections and interference between different parts compared with binary segmentation and instrument segmentation. The performance of SAM was tested using data from the official testing set, and the results were compared against those provided in the official report. To better visualize, segmentation results of different categories have

Table 7. Zero-Shot Segmentation Results of SAM on Different MRI Organ Classes in AMOS Dataset

Class	Dice	IoU
#1	0.2571	0.1785
#2	<b>0.4622</b>	<b>0.3866</b>
#3	0.4434	0.3656
#4	0.1437	0.1026
#5	0.0352	0.0207
#6	0.4480	0.3311
#7	0.1475	0.0912
#8	0.2843	0.2285
#9	0.0691	0.0452
#10	0.1175	0.0754
#11	0.0054	0.0027
#12	0.0243	0.0177
#13	0.0989	0.0642
Average	0.2264	0.1723

Table 8. Quantitative Results of Zero-Shot SAM in X-Ray Dataset

Method	Dice	IoU
SAM	0.6509	0.5136

Table 9. Comparison with the State-of-the-Art Methods on MIC-CAI 2017 Robotic Instrument Segmentation Datasets

Method	Class	Dice	IoU
UNet [27]	All	0.6075	0.4841
TernausNet-16 [28]	All	<b>0.7597</b>	<b>0.6550</b>
TernausNet-11 [28]	All	0.7425	0.6223
LinkNet-34 [28]	All	0.4126	0.3455
SAM	Clasper	0.4296	0.3054
	Wrist	0.5076	0.3674
	Shaft	0.7189	0.5076
	All	0.5512	0.4227

been plotted onto the same graph for comparison, which are shown in both Figure 1 (E) and Figure 2 (E). It should be noted that even though some examples exhibit visually satisfactory results, which may be because the predicted results of some categories overlap with each other. From a quantitative perspective as shown in Table 9, SAM has already surpassed the segmentation performance of LinkNet-34 [7, 28] by only receiving prompts. However, it is still not comparable to the current SOTA and there is a 30% relative gap between SAM and the SOTA method.

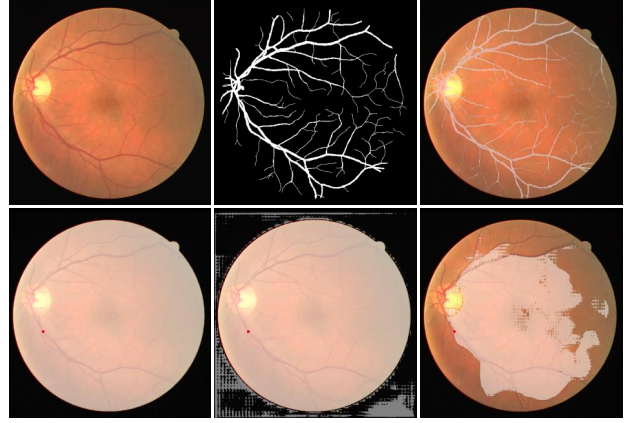


Figure 3. A failure sample of SAM on segmenting retinal vessels. The first row from left to right is: the initial input image, ground truth mask, and the input image superimposed with the ground truth mask. The second row from left to right shows three different segmented images by SAM, with the score of 1.007, 0.993, and 0.673, respectively.

### 3.3.9 Retinal Vessel Images

We also used SAM to segment vessels. However, the experiments revealed that zero-shot SAM was not able to accurately segment blood vessels in retinal images, despite the *manual* provision of additional prompts focused on areas where vessel visibility is pronounced. At the current stage, we conjectured that the segmentation of continuously branching structures, such as blood vessels and tree branches, presents a challenge for SAM. From Figure 3. Within the fundus image, it was observed that SAM encountered difficulties in accurately identifying blood vessels as distinct segmentable objects. Nevertheless, after fine-tuning SAM, a significant improvement in vessel segmentation can be observed as illustrated in Figure 4. The segmentation results of SAM after fine-tuning almost perfectly match with ground truth, with only a bit of missing parts at the terminal ends of the vessels (SAM ViT-B was fine-tuned in this experiment), which shows the potential of SAM for precise medical segmentation by domain-specific fine-tuning.

## 4. Discussion

Through extensive experiments, it was found that SAM was unable to outperform models specially designed for medical imaging by simply using its zero-shot feature. It is worth noting that SAM was trained primarily on natural images and had limited access to diverse medical modalities containing pathological manifestations. As such, the medical segmentation results obtained using SAM’s zero-shot capability were actually decent and sometimes considered impressive as shown in Figure 1. Nevertheless, given prompts in the same way, the performance of SAM

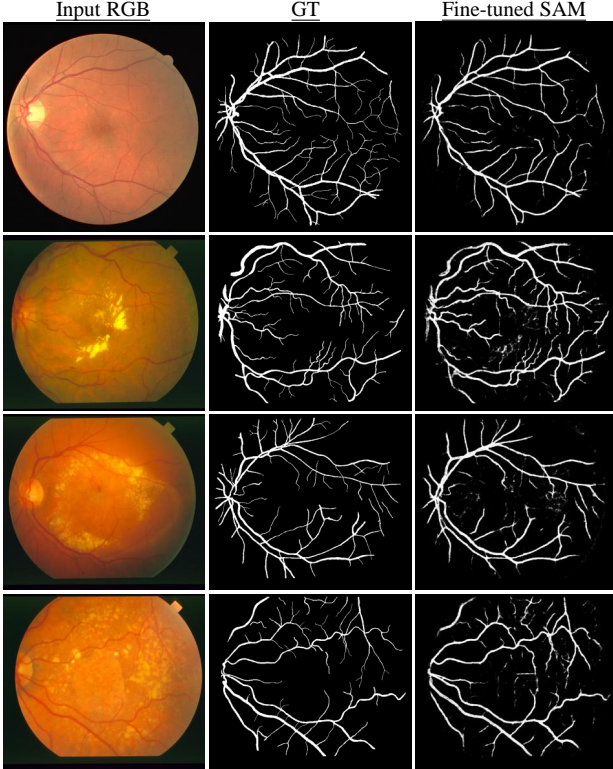


Figure 4. Segmentation samples of SAM fine-tuned on retinal vessels. Each row from left to right is the initial input image, ground truth mask and prediction of fine-tuned SAM. The column from top to bottom shows four different retinal images from different datasets.

varies significantly across different medical modalities. In endoscopy and dermoscopy, SAM demonstrated better performance compared to other medical modalities. In segmenting a skin lesion, if there are no clear boundaries in the pathological morphology or if the skin itself has pigment deposition and erythematosis, the segmentation outcome of SAM is often unsatisfactory. This phenomenon resembles the concealed patterns observed in natural images, which have been previously shown to be a challenge for SAM [17, 31]. Although the retinal fundus images are also RGB images, segmenting structural targets within the internal structure of the eye is not encountered in natural scenes. This has resulted in suboptimal optic disc segmentation and complete failure in retinal vessel segmentation of SAM using zero-shot segmentation.

Despite the SA-1B dataset used for training SAM containing 1B masks and 11M images, the multiple medical domains we tested in the case study are entirely unseen domains for SAM. Especially in medical imaging, 3D imaging predominates as a critical methodology, such as MRI, CT, and OCT. The 2D slices employed for analysis are an

unique aspect of medical imaging and cannot be found in natural domain. For instance, features of OCT B-scan are layered structures stretching along the entire image width, instead of closed regions. Algorithms developed specifically for the prominent features of OCT have demonstrated excellent performance [1, 33]. However, SAM is unable to discriminate the tissue and features in OCT images without any prior knowledge. Furthermore, vessels that spread throughout the whole retinal fundus image are difficult for SAM to segment in a zero-shot manner as shown in Figure 3. Besides the presence of domain differences between medical and natural images, it has been observed in Table 3 that SAM exhibited significant imbalanced segmentation accuracy when encountering different domain images under the same category.

To evaluate the capabilities of SAM under zero-shot settings, experiments of this study used a single prompt selection method and provided the center point of the ground truth mask as the prompt for each sample. Although this approach did not fully harness the potential of SAM, it sufficed to highlight the limitations of SAM in some specific medical scenarios. Recently, SAM-Adapter [9] has been proposed for confusing scenario segmentation on natural image datasets including but not limited to camouflaged targets and defocus blur objects, which has shown better results than SAM and other task-specific approaches. Medical images can be regarded as a distinct category of rare scenes. Consequently, it is very likely that natural image-based large models after fine-tuning may yield excellent performance for medical modalities as revealed by our preliminary results of SAM fine-tuned on retinal vessel data. Meanwhile, different prompt engineering techniques can be further explored. Furthermore, it is worth investigating if training a large medical vision model from scratch using only medical data can lead to better performance than continual-training/fine-tuning a large vision model on medical data, which has been previously pretrained on large volume of natural image data.

During the development phase of large medical AI models, it is recommended to prioritize a focus on diagnostic information and invariant features present in medical images. This can potentially mitigate issues related to domain transfer, thus enhancing the overall performance and interpretability of a large AI model.

## 5. Conclusions

This work presents a case study of the Segment Anything Model on a wide range of zero-shot medical image segmentation tasks. Through comprehensive experiments, we identified the challenges that SAM currently encounters in this context. Importantly, our analysis was performed on a standardized set of prompts devoid of any prior medical knowledge, covering a diverse range of imaging modalities,



such as dermoscope, fundus, CT, MRI, endoscope, X-Ray, endoscopic OCT and spectral domain OCT. The provision of precise and interactive prompts, the use of specialized feature extraction methodologies tailored for medical images, and the well-designed fine-tuning of large vision models originally trained on natural images can be explored in future work. Given the unique challenges associated with medical imaging, these aspects are critical for ensuring the optimal performance of generalist models within this domain. Additionally, it is crucial that large medical vision models possess cross-domain generalizability, akin to that exhibited by physicians. This is important to avoid any negative impact on diagnostic accuracy resulting from the replacement of data acquisition equipment and protocols. Overall, our findings highlight the need for a medical foundation model, with careful consideration given to the specific challenges posed by this complex and rapidly evolving field.

## References

- [1] Sai Mu Dalike Abaxi, Mehmood Nawaz, Peilun Shi, Hao Wei, Syeda Aimen Abbasi, and Wu Yuan. Lideoctnet: A lightweight oct-aware framework for segmentation of irregularly layered tissue structures. 2023. 6, 8
- [2] Max Allan, Alex Shvets, Thomas Kurmann, Zichen Zhang, Rahul Duggal, Yun-Hsuan Su, Nicola Rieke, Iro Laina, Niveditha Kalavakonda, Sebastian Bodenstedt, et al. 2017 robotic instrument segmentation challenge. *arXiv preprint arXiv:1902.06426*, 2019. 2, 3
- [3] Marin Benčević, Irena Galić, Marija Habijan, and Danilo Babin. Training on polar image transformations improves biomedical image segmentation. *IEEE Access*, 9:133365–133375, 2021. 4
- [4] Rishi Bommasani, Drew A Hudson, Ehsan Adeli, Russ Altman, Simran Arora, Sydney von Arx, Michael S Bernstein, Jeannette Bohg, Antoine Bosselut, Emma Brunskill, et al. On the opportunities and risks of foundation models. *arXiv preprint arXiv:2108.07258*, 2021. 1
- [5] Sema Candemir, Stefan Jaeger, Kannappan Palaniappan, Jonathan P Musco, Rahul K Singh, Zhiyun Xue, Alexandros Karargyris, Sameer Antani, George Thoma, and Clement J McDonald. Lung segmentation in chest radiographs using anatomical atlases with nonrigid registration. *IEEE transactions on medical imaging*, 33(2):577–590, 2013. 2, 3, 6
- [6] Fabio M Carlucci, Antonio D’Innocente, Silvia Bucci, Barbara Caputo, and Tatiana Tommasi. Domain generalization by solving jigsaw puzzles. In *Proceedings of the IEEE/CVF Conference on Computer Vision and Pattern Recognition*, pages 2229–2238, 2019. 6
- [7] Abhishek Chaurasia and Eugenio Culurciello. Linknet: Exploiting encoder representations for efficient semantic segmentation. In *2017 IEEE visual communications and image processing (VCIP)*, pages 1–4. IEEE, 2017. 7
- [8] Jieneng Chen, Yongyi Lu, Qihang Yu, Xiangde Luo, Ehsan Adeli, Yan Wang, Le Lu, Alan L Yuille, and Yuyin Zhou. Transunet: Transformers make strong encoders for medical image segmentation. *arXiv preprint arXiv:2102.04306*, 2021. 4, 6
- [9] Tianrun Chen, Lanyun Zhu, Chaotao Ding, Runlong Cao, Shangzhan Zhang, Yan Wang, Zejian Li, Lingyun Sun, Papa Mao, and Ying Zang. Sam fails to segment anything? – sam-adapter: Adapting sam in underperformed scenes: Camouflage, shadow, and more, 2023. 8
- [10] Noel Codella, Veronica Rotemberg, Philipp Tschandl, M Emre Celebi, Stephen Dusza, David Gutman, Brian Helba, Aadi Kalloo, Konstantinos Liopyris, Michael Marchetti, et al. Skin lesion analysis toward melanoma detection 2018: A challenge hosted by the international skin imaging collaboration (isic). *arXiv preprint arXiv:1902.03368*, 2019. 2, 3
- [11] Ruining Deng, Can Cui, Quan Liu, Tianyuan Yao, Lucas W Remedios, Shunxing Bao, Bennett A Landman, Lee E Wheless, Lori A Coburn, Keith T Wilson, et al. Segment anything model (sam) for digital pathology: Assess zero-shot segmentation on whole slide imaging. *arXiv preprint arXiv:2304.04155*, 2023. 1
- [12] Bo Dong, Wenhai Wang, Deng-Ping Fan, Jinpeng Li, Huazhu Fu, and Ling Shao. Polyp-pvt: Polyp segmentation with pyramid vision transformers. *arXiv preprint arXiv:2108.06932*, 2021. 4
- [13] Deng-Ping Fan, Ge-Peng Ji, Tao Zhou, Geng Chen, Huazhu Fu, Jianbing Shen, and Ling Shao. Pranet: Parallel reverse attention network for polyp segmentation. In *Medical Image Computing and Computer Assisted Intervention—MICCAI 2020: 23rd International Conference, Lima, Peru, October 4–8, 2020, Proceedings, Part VI* 23, pages 263–273. Springer, 2020. 4
- [14] Francisco Fumero, Silvia Alayón, José L Sanchez, Jose Sigut, and M Gonzalez-Hernandez. Rim-one: An open retinal image database for optic nerve evaluation. In *2011 24th international symposium on computer-based medical systems (CBMS)*, pages 1–6. IEEE, 2011. 2, 3
- [15] Stefan Jaeger, Alexandros Karargyris, Sema Candemir, Les Folio, Jenifer Siegelman, Fiona Callaghan, Zhiyun Xue, Kannappan Palaniappan, Rahul K Singh, Sameer Antani, et al. Automatic tuberculosis screening using chest radiographs. *IEEE transactions on medical imaging*, 33(2):233–245, 2013. 2, 3, 6
- [16] Debesh Jha, Michael A Riegler, Dag Johansen, Pål Halvorsen, and Håvard D Johansen. Doubleu-net: A deep convolutional neural network for medical image segmentation. In *2020 IEEE 33rd International symposium on computer-based medical systems (CBMS)*, pages 558–564. IEEE, 2020. 4
- [17] Ge-Peng Ji, Deng-Ping Fan, Peng Xu, Ming-Ming Cheng, Bowen Zhou, and Luc Van Gool. Sam struggles in concealed scenes—empirical study on “segment anything”. *arXiv preprint arXiv:2304.06022*, 2023. 8
- [18] Wei Ji, Jingjing Li, Qi Bi, Wenbo Li, and Li Cheng. Segment anything is not always perfect: An investigation of sam on different real-world applications. *arXiv preprint arXiv:2304.05750*, 2023. 1

- [19] Yuanfeng Ji, Haotian Bai, Jie Yang, Chongjian Ge, Ye Zhu, Ruimao Zhang, Zhen Li, Lingyan Zhang, Wanling Ma, Xiang Wan, et al. Amos: A large-scale abdominal multi-organ benchmark for versatile medical image segmentation. *arXiv preprint arXiv:2206.08023*, 2022. 2, 3, 5
- [20] Alexander Kirillov, Eric Mintun, Nikhila Ravi, Hanzi Mao, Chloe Rolland, Laura Gustafson, Tete Xiao, Spencer Whitehead, Alexander C Berg, Wan-Yen Lo, et al. Segment anything. *arXiv preprint arXiv:2304.02643*, 2023. 1
- [21] Ange Lou, Shuyue Guan, Hanseok Ko, and Murray H Loew. Caranet: context axial reverse attention network for segmentation of small medical objects. In *Medical Imaging 2022: Image Processing*, volume 12032, pages 81–92. SPIE, 2022. 4
- [22] Martina Melinščak, Marin Radmilović, Zoran Vatauvuk, and Sven Lončarić. Annotated retinal optical coherence tomography images (aroi) database for joint retinal layer and fluid segmentation. *Automatika*, 62(3-4):375–385, 2021. 2, 3
- [23] M Melinščak, M Radmilović, Zoran Vatauvuk, and S Lončarić. Aroi: Annotated retinal oct images database. In *2021 44th International Convention on Information, Communication and Electronic Technology (MIPRO)*, pages 371–376. IEEE, 2021. 5
- [24] José Ignacio Orlando, Huazhu Fu, João Barbosa Breda, Karel Van Keer, Deepti R Bathula, Andrés Diaz-Pinto, Ruogu Fang, Pheng-Ann Heng, Jeyoung Kim, JoonHo Lee, et al. Refuge challenge: A unified framework for evaluating automated methods for glaucoma assessment from fundus photographs. *Medical image analysis*, 59:101570, 2020. 2, 3
- [25] Hyeon-Cheol Park, Jessica Mavadia-Shukla, Wu Yuan, Milad Alemohammad, and Xingde Li. Broadband rotary joint for high-speed ultrahigh-resolution endoscopic oct imaging at 800 nm. *Optics letters*, 42(23):4978–4981, 2017. 2, 3, 5
- [26] Jianing Qiu, Lin Li, Jiankai Sun, Jiachuan Peng, Peilun Shi, Ruiyang Zhang, Yinzhaodong, Kyle Lam, Frank P-W Lo, Bo Xiao, Wu Yuan, Dong Xu, and Benny Lo. Large ai models in health informatics: Applications, challenges, and the future. *arXiv preprint arXiv:2303.11568*, 2023. 1
- [27] Olaf Ronneberger, Philipp Fischer, and Thomas Brox. U-net: Convolutional networks for biomedical image segmentation. In *Medical Image Computing and Computer-Assisted Intervention–MICCAI 2015: 18th International Conference, Munich, Germany, October 5-9, 2015, Proceedings, Part III 18*, pages 234–241. Springer, 2015. 4, 6, 7
- [28] Alexey A Shvets, Alexander Rakhlin, Alexandr A Kalinin, and Vladimir I Iglovikov. Automatic instrument segmentation in robot-assisted surgery using deep learning. In *2018 17th IEEE International Conference on Machine Learning and Applications (ICMLA)*, pages 624–628, 2018. 6, 7
- [29] Jayanthi Sivaswamy, S Krishnadas, Arunava Chakravarty, G Joshi, A Syed Tabish, et al. A comprehensive retinal image dataset for the assessment of glaucoma from the optic nerve head analysis. *JSM Biomedical Imaging Data Papers*, 2(1):1004, 2015. 2, 3
- [30] Feilong Tang, Qiming Huang, Jinfeng Wang, Xianxu Hou, Jionglong Su, and Jingxin Liu. Duat: Dual-aggregation transformer network for medical image segmentation. *arXiv preprint arXiv:2212.11677*, 2022. 4
- [31] Lv Tang, Haoke Xiao, and Bo Li. Can sam segment anything? when sam meets camouflaged object detection. *arXiv preprint arXiv:2304.04709*, 2023. 8
- [32] Philipp Tschandl, Cliff Rosendahl, and Harald Kittler. The ham10000 dataset, a large collection of multi-source dermatoscopic images of common pigmented skin lesions. *Scientific data*, 5(1):1–9, 2018. 2, 3
- [33] Ignacio A Viedma, David Alonso-Caneiro, Scott A Read, and Michael J Collins. Deep learning in retinal optical coherence tomography (oct): A comprehensive survey. *Neurocomputing*, 2022. 8
- [34] Shujun Wang, Lequan Yu, Kang Li, Xin Yang, Chi-Wing Fu, and Pheng-Ann Heng. Dofe: Domain-oriented feature embedding for generalizable fundus image segmentation on unseen datasets. *IEEE Transactions on Medical Imaging*, 2020. 4, 5, 6
- [35] Wu Yuan, Yan Feng, Defu Chen, Payam Gharibani, Jiande DZ Chen, Huimin Yu, and Xingde Li. In vivo assessment of inflammatory bowel disease in rats with ultrahigh-resolution colonoscopic oct. *Biomedical optics express*, 13(4):2091–2102, 2022. 5
- [36] Hongyi Zhang, Moustapha Cisse, Yann N Dauphin, and David Lopez-Paz. mixup: Beyond empirical risk minimization. *arXiv preprint arXiv:1710.09412*, 2017. 6
- [37] Ling Zhang, Xiaosong Wang, Dong Yang, Thomas Sanford, Stephanie Harmon, Baris Turkbey, Holger Roth, Andriy Myronenko, Daguang Xu, and Ziyue Xu. When unseen domain generalization is unnecessary? rethinking data augmentation. *arXiv preprint arXiv:1906.03347*, 2019. 6
- [38] Yundong Zhang, Huiye Liu, and Qiang Hu. Transfuse: Fusing transformers and cnns for medical image segmentation. In *Medical Image Computing and Computer Assisted Intervention–MICCAI 2021: 24th International Conference, Strasbourg, France, September 27–October 1, 2021, Proceedings, Part I 24*, pages 14–24. Springer, 2021. 4
- [39] Zongwei Zhou, Md Mahfuzur Rahman Siddiquee, Nima Tajbakhsh, and Jianming Liang. Unet++: A nested u-net architecture for medical image segmentation. In *Deep Learning in Medical Image Analysis and Multimodal Learning for Clinical Decision Support: 4th International Workshop, DLMIA 2018, and 8th International Workshop, ML-CDS 2018, Held in Conjunction with MICCAI 2018, Granada, Spain, September 20, 2018, Proceedings 4*, pages 3–11. Springer, 2018. 4